



HAL
open science

Rational direct synthesis of $[\text{Fe}(\text{Htrz})_2(\text{trz})](\text{BF}_4)$ polymorphs: temperature and concentration effects

Marlène Palluel, Liza El Khoury, Nathalie Daro, Sonia Buffiere, Michaël Josse, Mathieu Marchivie, Guillaume Chastanet

► To cite this version:

Marlène Palluel, Liza El Khoury, Nathalie Daro, Sonia Buffiere, Michaël Josse, et al.. Rational direct synthesis of $[\text{Fe}(\text{Htrz})_2(\text{trz})](\text{BF}_4)$ polymorphs: temperature and concentration effects. *Inorganic Chemistry Frontiers*, 2021, 8 (15), pp.3697-3706. 10.1039/D1QI00482D . hal-03304287

HAL Id: hal-03304287

<https://hal.science/hal-03304287v1>

Submitted on 28 Jul 2021

HAL is a multi-disciplinary open access archive for the deposit and dissemination of scientific research documents, whether they are published or not. The documents may come from teaching and research institutions in France or abroad, or from public or private research centers.

L'archive ouverte pluridisciplinaire **HAL**, est destinée au dépôt et à la diffusion de documents scientifiques de niveau recherche, publiés ou non, émanant des établissements d'enseignement et de recherche français ou étrangers, des laboratoires publics ou privés.

Rational direct synthesis of $[\text{Fe}(\text{Htrz})_2(\text{trz})](\text{BF}_4)$ polymorphs: temperature and concentration effects.

Marlène Palluel^a, Liza El Khoury^a, Nathalie Daro^a, Sonia Buffière^a, Michael Josse^a, Mathieu Marchivie^{*a}, Guillaume Chastanet^{*a}

Received 00th January 20xx,
Accepted 00th January 20xx

DOI: 10.1039/x0xx00000x

The $[\text{Fe}(\text{Htrz})_2(\text{trz})](\text{BF}_4)$ compound is probably the most studied in the spin crossover (SCO) community since it exhibits switching properties with a large temperature range of memory effect, just above room temperature. We present in this paper a detailed study of the influence of the synthetic parameters on the polymorphism of this compound. While the crystal structure of polymorph I is already known, we report the one of polymorph II and discuss the differences to allow further studies to discriminate between both. This was achieved through the resolution of the crystal structure of the $[\text{Fe}(\text{Htrz})_2(\text{trz})](\text{PF}_6)$ analog. This study allows to draw a phase diagram and to discuss the effect of the reaction conditions on the formation of polymorphs, the size of the particles and the properties.

Introduction

Over the past decades, the number of data created and stored is increasing day by day. To support this growth, there is a strong need for new data treatment units together with the minimizing of their size to enhance the amount of efficient operations in a reduced space. For such purpose, spin crossover systems are highly investigated due to their ability to store information down to the nanoscale^{1–3}. The magnetic, mechanic, electronic properties of Spin Crossover (SCO) materials can be switched by external stimuli such as temperature, pressure, light irradiation, electric field^{4–9}. This switching follows from the coexistence of two distinct states: high spin (HS) and low spin (LS). The reversible $\text{LS} \leftrightarrow \text{HS}$ transition is of particular interest for data storage application since it can occur with memory effect through the appearance of hysteresis cycles. For that purpose, the synthesis of SCO nanoparticles (NPs) has been deeply investigated^{3,10–12}.

Among SCO materials that can be processed at the nanometer scale, while keeping the properties they exhibit at the macroscopic scale, much attention has been driven toward polymeric triazole-based Fe(II) complexes¹⁰, and more specifically the $[\text{Fe}(\text{Htrz})_2(\text{trz})](\text{BF}_4)$ derivative. This compound has been widely studied since its discovery in 1977¹³ mainly because it exhibits a well-defined and large hysteresis cycle above room temperature. Two forms of this compound have been reported on the basis of magnetic properties¹⁴. The first one, called **1a**, shows a large hysteresis of ca. 40 K centred at 370 K and the second one, named **1b**, presents a narrower hysteresis of ca. 15 K, centred at 330 K. It is still not clear what differentiates both forms and if the variance between the two forms **1a** and **1b** can be linked to the existence of polymorphism as there is no structural information about form **1b**. The fact

that they are structural polymorphs is not established to date. The crystal structure of **1a** has been recently elucidated from powder X-Ray diffraction showing a one dimensional arrangement of $[\text{Fe}(\text{Htrz})_2(\text{trz})]^+$ chains separated by BF_4^- anions¹⁵. Many efforts have been devoted to the synthesis of NPs of this compound, following two main synthetic routes³. The first one is the *micellar synthesis*, allowing to get well shaped and nanosized particles, down to 5 nm^{16,17}. This approach requires the use of surfactants, such as neutral Tergitol NP9 or KBE3 (or Triton-100) or anionic NaAOT (bis(2-ethylhexyl)sulfosuccinate sodium salt), that can remain in the final material. In most cases, form **1a** is obtained following such approach. The second synthetic route to obtain NPs is the *direct synthesis* for which the control over the phase, the size and the shape of the particles is usually difficult. Except few examples no clear studies have been devoted to the rational direct synthesis of NPs of this phase¹⁸. However, this is a surfactant-free synthesis that can be of importance in the integration into composites^{3,19,20} and hybrid nanomaterials^{21–23}, deserving then an in-depth investigation. Very recently, new approaches have been proposed for the direct synthesis of such triazole-based compounds, starting from metallic iron²⁴ or using mechano-chemistry²⁵ as well as surfactant-free synthesis like spray-drying²⁶ or flow chemistry coupled to supercritical fluids treatment^{27,28}.

The aim of this paper is to investigate the direct synthesis conditions to obtain NPs of the $[\text{Fe}(\text{Htrz})_2(\text{trz})](\text{BF}_4)$ in the appropriate phase. Moreover, the crystal structure of phase **1b** is proposed from the study of the analogue $[\text{Fe}(\text{Htrz})_2(\text{trz})](\text{PF}_6)$, what supports the structural polymorphic nature of both forms. We propose then to rename form **1a** and **1b** to polymorph I and II, respectively, to definitively clarify the crystallographic polymorphic nature of these different forms. The target of this work is to clearly identify the synthetic conditions to obtain surfactant-free nanoparticles of the appropriate polymorph. Going further, it will provide all the elements to discriminate between both polymorphs and prevent misinterpretations as sometimes encountered in the literature.

^a University of Bordeaux, ICMCB, UMR 5026, 87 Avenue du Dr A. Schweitzer, F-33608 Pessac, France.

† Footnotes relating to the title and/or authors should appear here.

Electronic Supplementary Information (ESI) available: [magnetic and crystallographic data. CCDC numbers 2076931 (PF₆) and 2076943 (II)]. See DOI: 10.1039/x0xx00000x

Experimental

Material

All the chemicals and solvents were used as purchased from Sigma-Aldrich. For the synthesis of $[\text{Fe}(\text{Htrz})_2(\text{trz})](\text{BF}_4)$, the iron salt ($\text{Fe}(\text{BF}_4)_2 \cdot 6\text{H}_2\text{O}$; 97 %), the triazole (1*H*-1,2,4-triazole, 98 %) and the ascorbic acid (99 %) were used. For the $[\text{Fe}(\text{Htrz})_2(\text{trz})](\text{PF}_6)$, the synthesis requires the use of potassium hexafluorophosphate (KPF_6 , 99 %) and of the iron sulfate ($\text{FeSO}_4 \cdot 7\text{H}_2\text{O}$; 99 %).

Synthesis procedure

The synthesis procedure followed for this study has been inspired by the previous report¹⁴. The reactants have been dissolved in a mixture of water – ethanol with 60 % of water and 40 % ethanol. This mixture was used because it has been shown to be the optimal conditions for the further synthesis of Au@SCO nanohybrids described elsewhere²². The synthesis consists in dissolving the iron salt ($\text{FeBF}_4 \cdot 6\text{H}_2\text{O}$) with few mg of ascorbic acid into 1.7 mL of this mixture on one side and the triazole (1*H*-1,2,4-triazole, Htrz) into 1.7 mL of the same solvent mixture on the other side. The two solutions were mixed with magnetic stirring and let to react during 15 min at the fixed reaction temperature. Then, the resulting mixture was let to cool down to room temperature during 1h45 still with magnetic stirring. Finally, the precipitate was separated by centrifugation (8 000 rcf – 4 min), then washed with water and twice with the same water – ethanol mixture. A starting concentration of Fe(II) was set at 1.2 M as previously described by Moulet¹⁶ and is noted C_1 . Starting from this concentration, both the reaction temperature and the initial concentration of Fe(II) (keeping a stoichiometric amount of Htrz) have been changed. The Fe(II) concentration was varied from 2.4 to 0.15 M at 0, 20, 50 and 80 °C. The compounds were obtained and noted C_aT_b . C corresponds to the concentration of Fe(II), and a the dilution factor related to the starting concentration $C_1 = 1.2 \text{ M}$; $C_{1/2}$ being $C_1/2$ (0.6 M)... T corresponds to the reaction temperature and b its value, like T_{20} for a reaction conducted at 20 °C. Sixteen compounds were obtained: C_2T_0 , C_2T_{20} , C_2T_{50} , C_2T_{80} , C_1T_0 , C_1T_{20} , C_1T_{50} , C_1T_{80} , $C_{1/2}T_{20}$, $C_{1/2}T_{50}$, $C_{1/3}T_{20}$, $C_{1/3}T_{50}$, $C_{1/4}T_{20}$, $C_{1/6}T_{20}$, $C_{1/8}T_0$, $C_{1/8}T_{20}$.

In addition, polymorphs **I** and **II** and $[\text{Fe}(\text{Htrz})_3](\text{BF}_4)_2 \cdot x\text{H}_2\text{O}$ (named **Htrz₃**) were synthesized strictly according to the procedure reported previously¹⁴ to have reference compounds, especially for powder X-Ray diffraction. Finally, the synthesis of $[\text{Fe}(\text{Htrz})_2(\text{trz})](\text{PF}_6)$ derivative (named **PF₆**) was adapted from a previously reported protocol²⁹ (see supplementary data). These 4 compounds were used to obtain structural and magnetic properties references.

Magnetic measurements

Magnetic measurements of the sixteen samples were performed using a MPMS-5S Quantum Design SQUID magnetometer operating at 5 kOe. The weighted powder sample ($\approx 5 \text{ mg}$) was inserted in a polypropylene bag which was sealed thereafter and put in a straw fixed to the sample holder

of the SQUID magnetometer. The diamagnetic contributions of the sample and the sample holder were removed from the data. The thermal cycles were performed at 0.7 K min^{-1} scan rate in settle mode for all the measurements. The procedure consisted in a first warming of the compound to 380 K inside the magnetometer and finally starting the measurement of two or three additional cycles (going back and forth from 300 to 380 K). For compounds presenting traces of Htrz₃ in their diffractograms, cycles were run between 200 and 380 K. The curves presented and discussed relate to the last stabilized cycle.

Powder X-ray diffraction

Powder X-ray diffractograms were acquired using a PANalytical X'Pert PRO MDP Powder diffractometers equipped with a Ge 111 monochromator using the θ -2 θ Bragg-Brentano geometry (Cu-K α 1 radiation, X'Celerator detector) or using the transmission capillary geometry equipped with a Goebel mirror (Cu-K α 1/2 radiations, X'Celerator detector) depending of the samples. More specifically the measurements were done using capillaries when too small amount of compound was obtained for some synthesis at low concentrations. Measurements were done from 5 ° to 60 ° (2 θ).

Transmission electron microscopy

Transmission electron microscopy (TEM) images were acquired using a JEOL 1400+ (Japan) with a tension of 60 kV. Each compound was analyzed separately and the measurements of 100 particles were done to give the average dimensions.

Scanning electron microscopy

Scanning electron microscopy (SEM) images were acquired using a JEOL 6700F (field emission gun). Experimental conditions were the followings: tension of 5 kV, working distance WD = 6 mm.

Results and discussion

Sixteen powders were synthesized at various temperatures and concentrations of reactants. In order to compare all these compounds and to identify the polymorphs, a detailed structural analysis was performed on reference compounds $[\text{Fe}(\text{Htrz})_2(\text{trz})](\text{BF}_4)$ -**I** and **II**, to evidence the differences between the two phases. In this discussion was also included the $[\text{Fe}(\text{Htrz})_3](\text{BF}_4)_2 \cdot x\text{H}_2\text{O}$ derivative that is sometimes found as a by-product. This compound exhibits a phase transition from phase α to phase β upon warming above 360 K, the α phase being the one obtained after synthesis and each of these phases having its own hysteresis curve¹⁴. Finally, the synthesis and crystallographic study of the $[\text{Fe}(\text{Htrz})_2(\text{trz})](\text{PF}_6)$ was helpful to solve the structure of polymorph **II** as described below.

The four diffractograms are presented in Figure 1. One can first clearly see that polymorphs **I** and **II** can be discriminated quite easily since around 11 °, **I** exhibits a doublet while **II** presents a single peak. However, it has to be mentioned that this view can be blurred at the nanoscale with a broadening of the peaks that

can merge the doublet in **I** into a wide shouldered singlet. Differences also appear around 25° with several peaks for **I** and less and broader peaks for **II**. Even if the crystallites sizes are much smaller in **II**, the differences in the diffractograms cannot be explained only by the broadening of the peaks, which positions must also be significantly different. Compound α -[Fe(Htrz)₃](BF₄)₂·xH₂O has a rich pattern with a very characteristic doublet at 7.9° and 8.3° and additional weaker peaks at 12.1° and 25.1° that will be useful to detect residual α -[Fe(Htrz)₃](BF₄)₂·xH₂O in other compounds. [Fe(Htrz)₂(trz)](PF₆) exhibits also a rich pattern with a doublet around 11° similar to **I** and several peaks between 15° and 25°. The unit cell parameter of this last compound have been determined from its well-defined diffractogram using the DICVOL06³⁰ software and then refined in the orthorhombic Pnma space group giving: *a* = 15,947(5) Å, *b* = 7,929(3) Å and *c* = 10,777(3) Å (with *V* = 1362,7(7) Å³). Compared to the known crystal structure of **I**, the PF₆ derivative shows thus similar cell parameters (accounting for the HS unit-cell parameters of **I**¹⁵) and the same space group despite significantly different diagrams. According to these similitudes the crystal structure of polymorph **I**, previously solved by Grosjean et al.¹⁵, was used as a starting point to solve that of [Fe(Htrz)₂(trz)](PF₆).

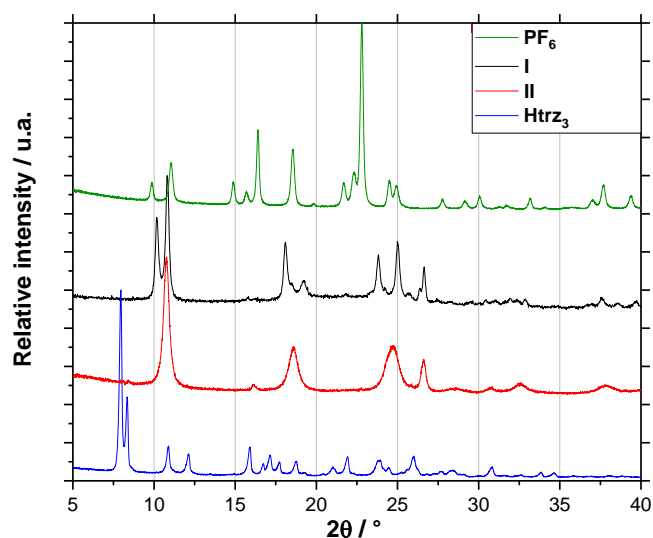


Figure 1: Powder X-Ray diffractograms for compounds [Fe(Htrz)₂(trz)](PF₆), [Fe(Htrz)₂(trz)](BF₄)-**I**, [Fe(Htrz)₂(trz)](BF₄)-**II** and α -[Fe(Htrz)₃](BF₄)₂·H₂O.

The crystal structure has been refined using a related model in which the BF₄⁻ anion has been replaced by the PF₆⁻ one. The three triazole heterocycles have been defined as rigid blocs at 120° from each other, the plans of the cycles being parallel to the *b* axis. The overall was let free to move forward and rotate around the *b* axis. The PF₆⁻ anion lies onto the mirror plane normal to *b* axis and is only free to move within this plane or rotate around the P-F bond parallel to the *b* axis.

A good concordance has been obtained between the calculated and the measured diffractograms (see Figure S12) with good agreement factor for molecular materials. This structure corresponds to the HS state (Figure S11) since the average Fe –

N distance refine to 2,217(10) Å which is superior to the one of the [Fe(Htrz)₂(trz)](BF₄)-**I** of 1,962(15) Å at room temperature (Table 1). This refinement allows the visualization of the crystal packing of the polymeric chains of the [Fe(Htrz)₂(trz)](PF₆). Concerning these triazole ligands in the crystal packing, Figure S13 clearly shows the alignment of the deprotonated triazole ligand along the crystallographic axis *a*. This alignment constitutes a noteworthy change with the [Fe(Htrz)₂(trz)](BF₄). Indeed, for this latter, the deprotonated triazole was located at -50,7° from the *a* axis. This strong rotation causes a modification of the interaction between the chains, four direct interactions for the [Fe(Htrz)₂(trz)](PF₆) against six for the [Fe(Htrz)₂(trz)](BF₄). Therefore, this rotation could explain the strong variation of the *a* and *c* parameters in [Fe(Htrz)₂(trz)](PF₆). Indeed, despite a bigger anion between the chains, the *a* parameter is much smaller for [Fe(Htrz)₂(trz)](PF₆), the decrease of the *a* parameter (and increase of *c*) could be related to the rotation of the [Fe(Htrz)₂(trz)]⁺ chains. Such structural modifications could also contribute to the modification of the magnetic properties between these two compounds (Figure S11).

In order to enlighten the structural differences between polymorph **I** and **II** of [Fe(Htrz)₂(trz)](BF₄), the cell parameters of polymorph-**II** have been refined by profile matching starting from those of polymorph **I**. The results lead to the orthorhombic cell parameters gathered in Table 1. A few conclusions can be made: i) the refinement results are good enough to trust this orthorhombic cell or a related monoclinic one with β close to 90°, ii) the found cell parameters are significantly different from those of polymorph **I**, especially concerning *a* and *c* parameters, keeping in mind that they are both in the LS state, and iii) the *b* parameter remains almost unchanged suggesting a similar crystal structure with [Fe(Htrz)₂(trz)]⁺ chains lying along the *b* axis in the low spin state. The first consequence of these observations is that the difference between the two forms of [Fe(Htrz)₂(trz)](BF₄) is not only due to different microstructure, but corresponds to a modification of the crystal structure clearly revealed by significant differences of *a* and *c* parameters compared to the polymorph **I**. These two forms are therefore structural polymorphs.

Table 1: Unit cell parameters and switching properties of polymorphs **I** and **II** of [Fe(Htrz)₂(trz)](BF₄), [Fe(Htrz)₂(trz)](PF₆).

Compounds (spin state) / Cell and magnetic parameters	I (LS)	II (LS)	PF₆ (HS)
Structure	Pnma	Pnma	Pnma
<i>a</i> (Å)	17.294(6)	16.691(4)	15.947(5)
<i>b</i> (Å)	7.337(2)	7.338(1)	7.929(2)
<i>c</i> (Å)	9.182(3)	9.482(3)	10.777(3)
<i>V</i> (Å ³)	1165.1(6)	1161.3(5)	1362.7(7)
<i>d</i> _{Fe-N} (Å)	1.962(15)	1.962(9)	2.217(10)
<i>T</i> _{1/2↑} (K)	376	354	278
<i>T</i> _{1/2↓} (K)	345	340	255
ΔT	31	14	23

The resolution of the $[\text{Fe}(\text{Htrz})_2(\text{trz})](\text{PF}_6)$ structure has brought a new perspective for the resolution of the $[\text{Fe}(\text{Htrz})_2(\text{trz})](\text{BF}_4)$ -II structure. Indeed, the refinement of its cell parameters leads to a similar trend than for $[\text{Fe}(\text{Htrz})_2(\text{trz})](\text{PF}_6)$ with a decrease of a and an increase of c . The structural difference between these two compounds probably comes from the rotation of the chains. According to these hypotheses, a structural model similar to that used for $[\text{Fe}(\text{Htrz})_2(\text{trz})](\text{PF}_6)$ has been used to perform a Rietveld refinement on polymorph II PXRD pattern. The results illustrated in Figure S14, shows satisfying agreement between the model shown on Figure 2 and the observed data.

As the calculated profile does not perfectly match the data we must consider this crystal structure for polymorph II as the most probable hypothesis. Indeed, according to the similitudes with the PF_6 derivative and the relatively well reproduced peak intensities, the true crystal structure should be close to this one. According to this model, the deprotonated triazole is located at $55,4^\circ$ from the a axis corresponding to a "rotation" of the chains of 106.1° between polymorph I and II (Figure 2). This "rotation" can also be explained by a 180° rotation of the BF_4^- accompanied by a slight rotation of 5° of the chains. It is worth to note that this structural modification can also be viewed as different deprotonated triazole ligand between I and II, it is then possible that the crystal structure of II consists of deprotonated triazoles at different positions leading to a more or less disordered structure.

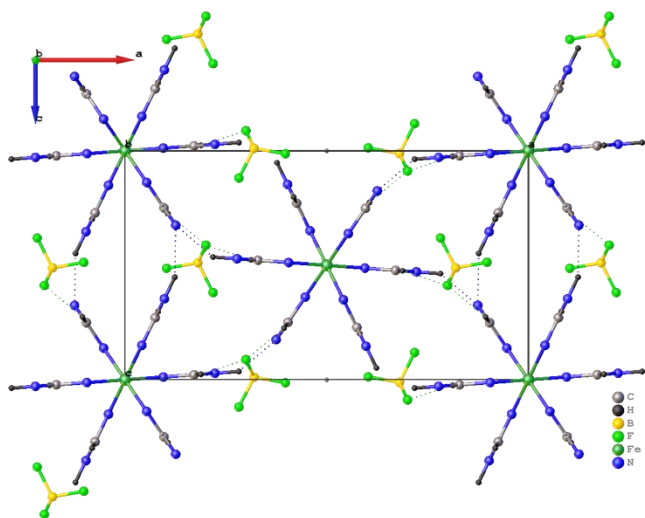


Figure 2: Crystal structure of II viewed along the b axis. Dotted lines represent direct short contacts between chains.

Since from powder X-ray patterns polymorphs I, II of $[\text{Fe}(\text{Htrz})_2(\text{trz})](\text{BF}_4)$ and α - $[\text{Fe}(\text{Htrz})_3](\text{BF}_4)_2 \cdot \text{H}_2\text{O}$ can be discriminated, the PXRD patterns of all the sixteen powders synthesized in the exploration of the temperature and concentration parameters effect were refined. The full table summarizing the various syntheses with all the corresponding characterizations is reported in supplementary material (Table S11). In the following, we will first discuss the effect of reactant concentration on the synthesis performed at 20°C (compounds C_aT_{20}) and secondly discuss the effect of temperature at C_1 .

Dilutions at 20°C

Seven syntheses with Fe(II) concentration going from 2.4 M to 0.15 M have been performed at the given temperature of 20°C . The thermal dependence of the χ_{MT} product (χ_{M} being the molar magnetic susceptibility) of these samples is presented in Figure 3 and the related data are detailed in Table 2. This compound is known to require at least one first run-in thermal cycle to reach stabilized properties (due to a loss of water or more probably (micro)structural modifications)^{14,16,31,32}, the curves presented correspond to the third and stabilized hysteresis cycle. All these samples exhibit a χ_{MT} value at 390 K around $3,2 \text{ cm}^3 \text{ K mol}^{-1}$ (except for the C_2T_{20} that is around $2.9 \text{ cm}^3 \text{ K mol}^{-1}$) consistent with the HS $S = 2$ configuration of the Fe(II). Upon cooling, a clear decrease of χ_{MT} down to around $0.5 - 0.75 \text{ cm}^3 \text{ K mol}^{-1}$ witnesses the occurrence of a spin crossover and the presence of a HS residue at low temperature which might be indicative of small particles sizes. All these samples exhibit a thermal hysteresis upon further warming, with a clear evolution of its width upon the samples: a widening of the hysteresis loop going from 14 to 32 K is observed from C_1T_{20} to $\text{C}_{1/8}\text{T}_{20}$ (Table 2). Three different behaviours stand out. The first one is characterized by a large hysteresis of 30 K ($T_{1/2\uparrow} \sim 375 \text{ K}$ and $T_{1/2\downarrow} \sim 340 \text{ K}$). This large hysteresis centred at 360 K, characteristic of polymorph $[\text{Fe}(\text{Htrz})_2(\text{trz})](\text{BF}_4)$ -I¹⁴, is obtained for the lowest concentrations of reactants $\text{C}_{1/4}\text{T}_{20}$, $\text{C}_{1/6}\text{T}_{20}$ and $\text{C}_{1/8}\text{T}_{20}$. The second behaviour is defined by a smaller hysteresis width ($\sim 15 \text{ K}$), with transition temperatures $T_{1/2\uparrow} = 360 \text{ K}$ and $T_{1/2\downarrow} = 340 \text{ K}$. These characteristics may correspond to polymorph $[\text{Fe}(\text{Htrz})_2(\text{trz})](\text{BF}_4)$ -II¹⁴ and are obtained for the compounds C_1T_{20} and $\text{C}_{1/2}\text{T}_{20}$. Finally, a third behaviour is observed for C_2T_{20} , with a two-step hysteresis. The first step is very similar to the one of polymorph II with $T_{1/2\uparrow} = 360 \text{ K}$ and $T_{1/2\downarrow} = 342 \text{ K}$ ($\Delta T = 18 \text{ K}$). The second step is very gradual going from 330 to 230 K and seems in agreement with the magnetic properties of the $[\text{Fe}(\text{Htrz})_3](\text{BF}_4)_2 \cdot x\text{H}_2\text{O}$ in its β phase¹⁴.

Table 2: Summary of the magnetic data of the samples synthesized at 20°C for Fe(II) concentrations going from 2.4 to 0.15 M. The phase listed first is the major phase as observed from PXRD.

Sample name	$T_{1/2\uparrow}$ (K)	$T_{1/2\downarrow}$ (K)	ΔT	phase
C_2T_{20}	360	342	18	II/ α -Htrz ₃
C_1T_{20}	354	340	14	II
$\text{C}_{1/2}\text{T}_{20}$	364	346	18	II/I
$\text{C}_{1/3}\text{T}_{20}$	373	344	29	II/I
$\text{C}_{1/4}\text{T}_{20}$	376	345	31	I/II
$\text{C}_{1/6}\text{T}_{20}$	378	346	32	I
$\text{C}_{1/8}\text{T}_{20}$	376	345	31	I

The diffractograms have also been recorded and are shown in Figure 3. A clear evolution of the structure from the compound C_1T_{20} to $\text{C}_{1/8}\text{T}_{20}$ can be observed. Indeed, the diffractogram obtained for the C_1T_{20} corresponds to polymorph II whereas for the $\text{C}_{1/8}\text{T}_{20}$ and $\text{C}_{1/6}\text{T}_{20}$ it corresponds to polymorph I.

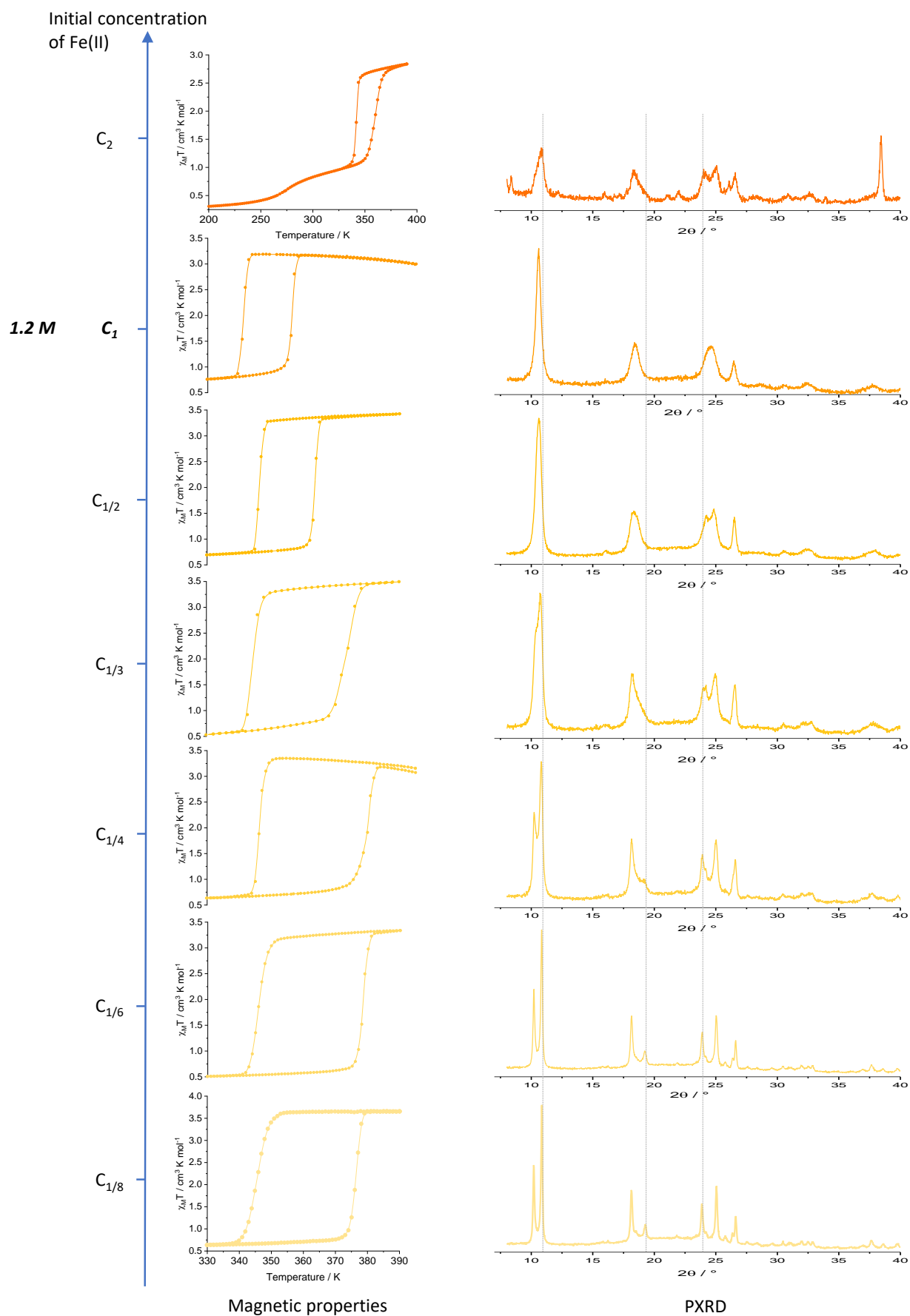


Figure 3: Thermal dependence of the $\chi_M T$ product recorded at 5 kOe at the temperature scan rate of 0.7 K/min (left) and Powder X-ray diffractograms (right) for the compounds synthesized at 20°C for concentrations going from 2.4 to 0.15 M of Fe(II).

Moreover, for the compound $C_{1/3}T_{20}$ the characteristic triplet of polymorph I is observed around 25° as well as the singlet around 12° from polymorph II. Thus, the $C_{1/3}T_{20}$ is a mixture of the two polymorphs I and II, as well as the compounds $C_{1/2}T_{20}$ and $C_{1/4}T_{20}$. As shown on the magnetic properties, compound $C_{2}T_{20}$ exhibits a diffractogram which differs from the other ones with features of polymorph II but also some of α - $[\text{Fe}(\text{Htrz})_3](\text{BF}_4)_2 \cdot x\text{H}_2\text{O}$ (peaks at 8.3° , 12.1° and 25.9°). These observations confirm the fact that the gradual conversion going from 230 to 330 K is coming from the β - $[\text{Fe}(\text{Htrz})_3](\text{BF}_4)_2 \cdot x\text{H}_2\text{O}$ obtained after warming at 380 K. Therefore, by only playing with the concentration of iron salt during the synthesis of $[\text{Fe}(\text{Htrz})_2(\text{trz})](\text{BF}_4)$, it is possible to master the obtaining of pure phases of both polymorphs I and II.

The morphology of each sample was analysed using Transmission and Scanning Electron Microscopies (Figures 4 and S15). The images of the compounds C_1T_{20} and $C_{1/2}T_{20}$ do not reveal any clear morphology, but show small particles (< 100 nm). On the contrary, from $C_{1/3}T_{20}$ to $C_{1/8}T_{20}$, clear rod-shaped particles are obtained and tend to stack into bigger agglomerates. This morphology is typical of phase I¹⁶ and it agrees with its presence evidenced by X-ray diffraction. The size of these rods evolves from around 120 nm to 500 nm along this series with more isolated particles while they are getting bigger.

Effect of temperature at C_1

At the given Fe(II) concentration of 1.2 M the temperature of the reaction was set at 0, 20, 50 and 80 °C. The thermal dependence of the $\chi_M T$ product of these four samples is presented in Figure 5 and the related data are detailed in Table 3. These four samples exhibit a $\chi_M T$ value $> 3 \text{ cm}^3 \text{ K mol}^{-1}$ at 390 K, consistent with the HS configuration of the Fe(II) in the structure. Upon cooling, a clear decrease of $\chi_M T$ down to around $0.5 - 0.75 \text{ cm}^3 \text{ K mol}^{-1}$ witnesses the occurrence of spin crossover and the presence of a small HS residue at low temperature which might be indicative of small particles sizes. All these samples exhibit a thermal hysteresis upon further warming, with a clear evolution of its width upon the samples. A widening of the hysteresis loop from 14 to 34 K, shifted toward higher temperatures, is observed going from compound C_1T_{20} to $C_{1/8}T_{20}$. This widening reveals an evolution from phase II of the $[\text{Fe}(\text{Htrz})_2(\text{trz})](\text{BF}_4)$ to phase I. However, compound C_1T_0 shows a larger hysteresis than C_1T_{20} with a $\Delta T = 30$ K, $T_{1/2\uparrow} = 372$ K and $T_{1/2\downarrow} = 342$ K (Figure 5).

The powder X-ray diffractograms of these four samples are reported on Figure 5. A clear evolution of the structure from polymorph II to I is observed from C_1T_{20} to $C_{1/8}T_{20}$. Compound C_1T_0 seems to correspond to polymorph II with some extra peaks revealing the presence of I (peak at 24°) and of $[\text{Fe}(\text{Htrz})_3](\text{BF}_4)_2 \cdot x\text{H}_2\text{O}$ in the sample (peaks at 15.8 ; 21.9 and 25.9° , even if small). The presence of the two polymorphs and $[\text{Fe}(\text{Htrz})_3](\text{BF}_4)_2 \cdot x\text{H}_2\text{O}$ in the same sample might explain the magnetic behaviour (Figure 5) even if there is no evidence of steps in the curve.

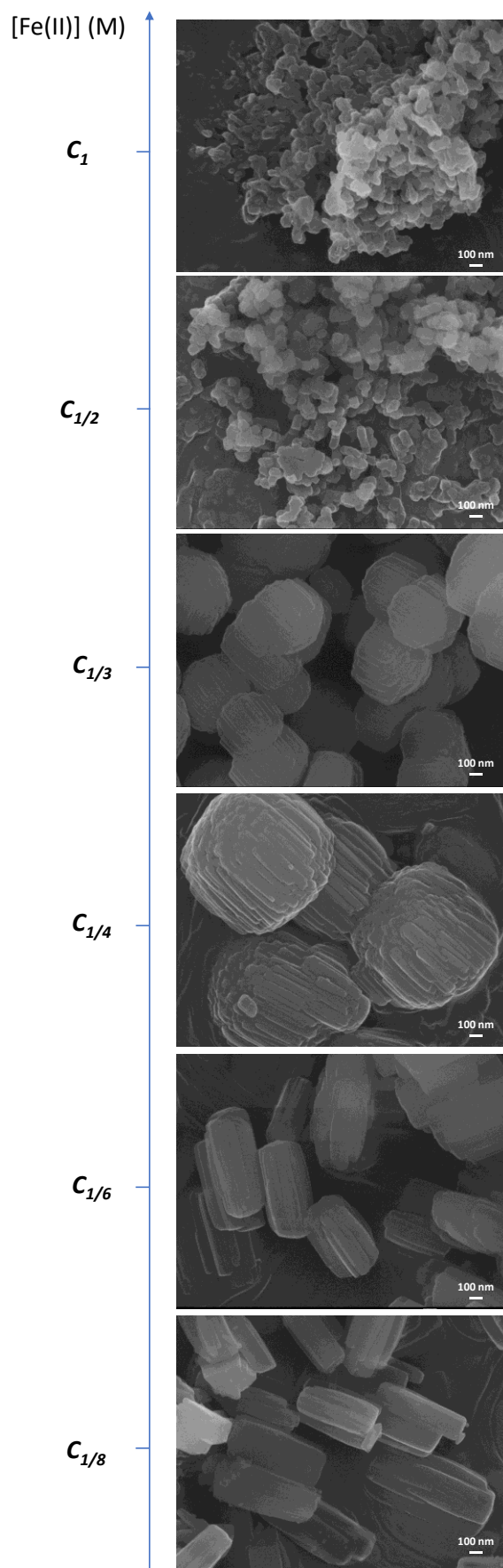


Figure 4: SEM pictures of the C_nT_{20} compounds.

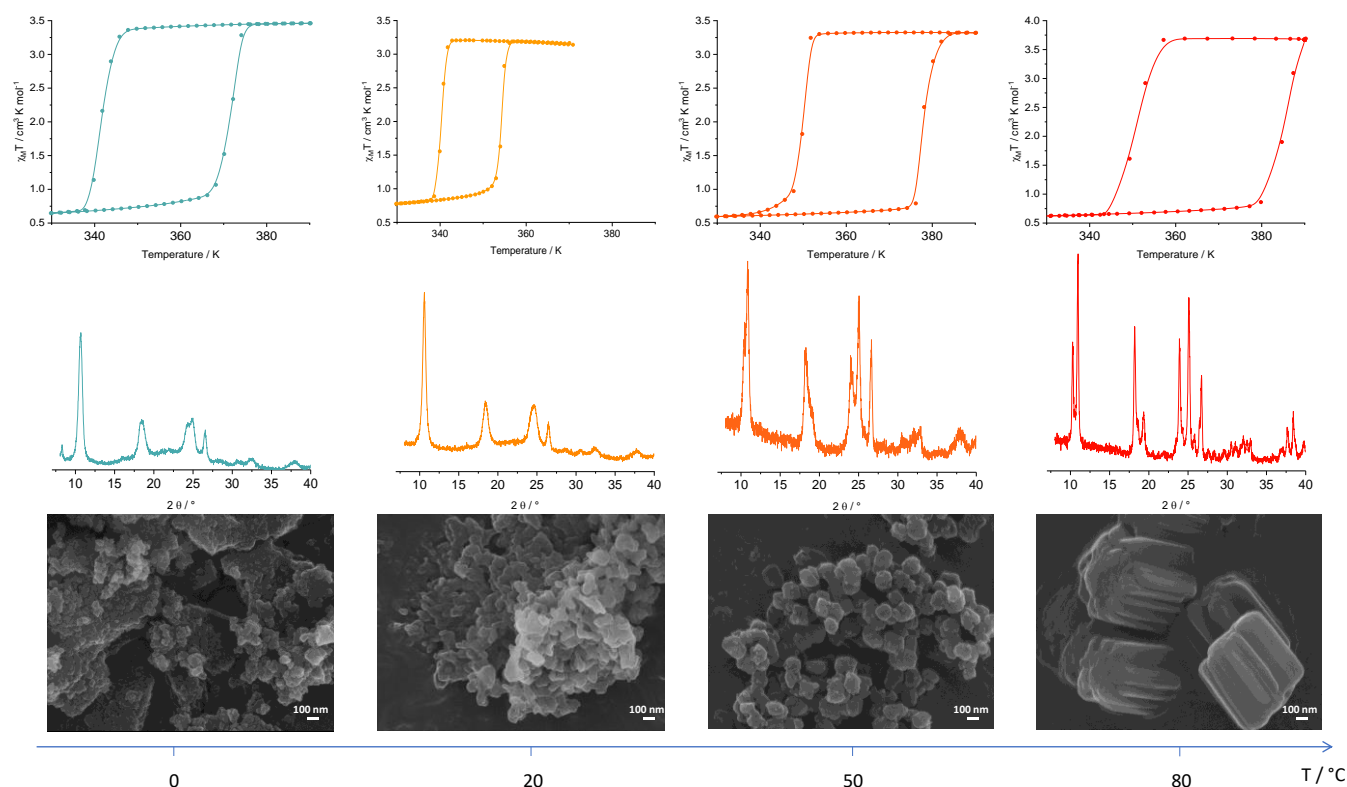


Figure 5: Thermal dependence of the $\chi_M T$ product recorded at 5 kOe at the temperature scan rate of 0.7 K/min (top) and Powder X-ray diffractograms (middle) and TEM images (bottom) for the compounds synthesized at 0, 20, 50 and 80 °C at a concentration of 1.2 M of Fe(II).

Table 3: Data of the compounds synthesized with 1.2 M of Fe(II) at various temperatures. The phase listed first is the major phase as observed from PXRD.

Sample name	$T_{1/2\uparrow}$ (K)	$T_{1/2\downarrow}$ (K)	ΔT	Phase
C_1T_0	372	342	30	II/I/Htrz ₃
C_1T_{20}	354	340	14	II
C_1T_{50}	378	350	28	I/II
C_1T_{80}	385	351	34	I

The morphology of each compound was analysed using Transmission and Scanning Electron Microscopies (Figures 5 and S15). C_1T_0 and C_1T_{20} do not present any clear morphology, with small particles (< 100 nm). On the contrary, for C_1T_{50} to C_1T_{80} , there are clear rod-shaped particles, typical of phase I¹⁶ and it agrees with its presence evidenced by X-ray crystallography.

Discussion

If we consider the other compounds synthesised in this study whose magnetic properties, powder X-ray diffractograms and TEM images are shown in Table S11 and Figure S15-7, clear trends can be drawn. A phase diagram for the synthesis of the $[\text{Fe}(\text{Htrz})_2(\text{trz})](\text{BF}_4)$ polymorphs can thus be set up (Figure 6). This diagram evidences that, polymorph I is favoured by high temperatures and low concentration of reactants. For high

concentrations, compound $[\text{Fe}(\text{Htrz})_3](\text{BF}_4)_2 \cdot x\text{H}_2\text{O}$ tends to co-crystallize with phases I and II. This is most probably due to more acidic conditions that prevent the deprotonation of the triazole ligand. These general observations can be completed by a clear distinction between phases in terms of morphology. Indeed, polymorph I shows well-defined particles with a cylindrical shape with size going from 500 to 1100 nm in length and from 250 to 700 nm in width, while polymorph II presents a non-defined morphology of particles, with random shape but in the nanoscale range below 200 nm. Such difference might come from the possible presence of disorder in the deprotonated triazole ligand in II, disfavoring its crystalline growth. Finally, a third morphology is observed on these images with anisotropic particles such as nanowires from 0.5 to 4 μm in length and 30 to 150 nm in width in compound $C_{1/8}T_0$. This sample corresponds mostly to the $[\text{Fe}(\text{Htrz})_3](\text{BF}_4)_2 \cdot x\text{H}_2\text{O}$ and constitutes an exception as for very low concentration, one do not expect its presence. Let us note also that these three morphologies can coexist in some samples in agreement with the structural and magnetic studies showing the presence of various phases in the same sample.

The overall crystallographic study brings important insights into the polymorphism of $[\text{Fe}(\text{Htrz})_2(\text{trz})](\text{BF}_4)$. Despite close powder X-ray diffraction patterns there are noticeable differences in the unit cell parameters. Indeed, while *b* does not change from I to II, *a* decreases and *c* increases by around 0.4 - 0.5 Å each. The unit cell volume is consequently bigger in I than in II. This

has a strong repercussion on data interpretation when studying the effect of grinding³³ or reaction conditions³⁴ for instance. In several cases, the change in the switching properties is not only coming from shaping and microstructural effects but mainly from polymorphism. A size reduction effect on the diffractogram of polymorph I cannot lead to a well-resolved singlet at 10.6 ° as in II but rather to a broad shouldered peak. The same comment can be made for the peaks around 18 °. The extraction of the unit cell parameters allows to discriminate between both phases and drive towards more reliable structure-properties relationships.

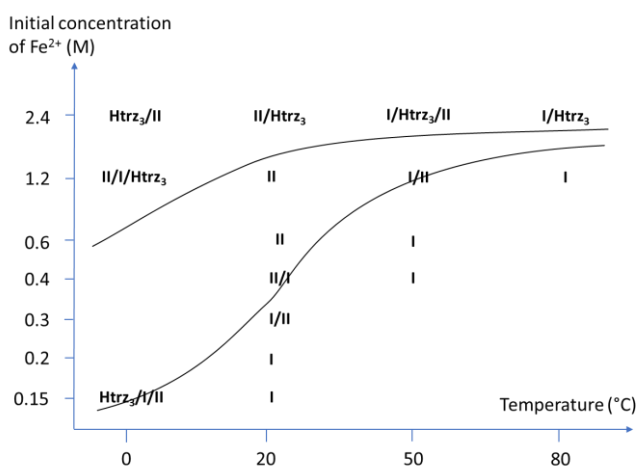


Figure 6: Phase diagram of $[\text{Fe}(\text{Htrz})_2(\text{trz})](\text{BF}_4)$ as function of synthesis conditions. The phase listed first is the major phase as estimated from PXRD.

Conclusions

With this study, a concentration/temperature phase diagram of the $[\text{Fe}(\text{Htrz})_2(\text{trz})](\text{BF}_4)$ has been drawn for the first time. This phase diagram (Figure 6) has clearly shown the impact of the synthesis condition on the obtained polymorphs. Moreover, it has revealed the difference in morphology between these polymorphs, with much more shaped particles for I than for II. Moreover, this study has shown definitively that both forms of $[\text{Fe}(\text{Htrz})_2(\text{trz})](\text{BF}_4)$ are structurally different and thus correspond to true polymorphs. Additionally the possible crystal structure of polymorph II has been proposed and therefore the differences in terms of crystal packing between both polymorphs are highlighted. This has been obtained with the help of the structure refinement of the $[\text{Fe}(\text{Htrz})_2(\text{trz})](\text{PF}_6)$, also solved for the first time. This diagram points out the difficulty to control by direct synthesis the phase, the morphology of the particles and the purity of the samples. There is no doubt this phase diagram will be very helpful for choosing synthesis conditions in the future. The study also allows to correlate the strong differences in the temperature, amplitude and shape of the SCO features observed between I and II to the differences in chains' organization and interchain interactions, although additional parameters (microstructure, particle size...) may be at play to favour these changes. The

accessibility of the crystal structure of both polymorphs is a clear asset to discriminate them, to evidence the role of such additional parameters and to finally draw reliable structure-properties relationships.

Conflicts of interest

There are no conflicts to declare.

Acknowledgements

CNRS, University of Bordeaux, Nouvelle Aquitaine Region and the ANR program (HEROES ANR-17-CE09-0010-01) are acknowledged for funding. The X-ray diffraction facility of the ICMCB is also thanked for the powder diffraction experiments and more particularly Eric Lebraud for the capillary measurements. The UMS PLACAMAT is acknowledged for the TEM facilities more specifically Marion Gayot for her help. MJ specifically thanks the CNRS for research delegation instrument.

Notes and references

- P. N. Martinho, C. Rajnak, M. Ruben, Nanoparticles, thin films and surface patterns from spin crossover materials and electrical spin state control, in *Spin-Crossover Materials: Properties and Applications*, 2013, John Wiley & Sons, Chichester, UK, 1st ed.
- K. Senthil Kumar, M. Ruben, *Coord. Chem. Rev.*, 2017, **346**, 176–205.
- L. Salmon, L. Catala, Spin crossover nanoparticles and nanocomposites materials, *C. R. Chim.*, 2018, **21**, 1–40.
- M. A. Halcrow, *Spin-Crossover Materials: Properties and Applications*, 2013, John Wiley & Sons.
- P. Gütllich and H. A. Goodwin, Spin crossover in transition metal compounds in *Top. Curr. Chem.* Springer., 2004, vol. 1, pp. 1–47.
- A. Bousseksou, N. Negre, M. Goiran, L. Salmon, J.-P. Tuchagues, M.-L. Boillot, K. Boukheddaden, F. Varret, Dynamic triggering of a spin transition by a pulsed magnetic field, *Eur. J. Phys. B*, 2000, **13**, 451–456.
- P. Gütllich, V. Ksenofontov, A. B. Gaspar, Pressure effect studies on spin crossover systems, *Coord. Chem. Rev.*, 2005, **249**, 1811–1829.
- E. Tailleur, M. Marchivie, J. P. Itié, P. Rosa, N. Daro, P. Guionneau, Pressure-induced spin crossover features at variable temperature revealed by in situ synchrotron powder X-ray diffraction, *Chem. - A Eur. J.*, 2018, **24**, 14495–14499.
- E. Collet, P. Guionneau, Structural analysis of spin crossover materials: from molecules to materials, *C. R. Chim.*, 2018, **21**, 1–19.
- O. Roubeau, Triazole-based one-dimensional spin crossover coordination polymers, *Chem. - A Eur. J.*, 2012, **18**, 15230–15244.
- J.-F. Létard, P. Guionneau, L. Goux-Capes, *Top. Curr. Chem.*, 2004, **1**, 221–249.
- A. Grosjean, P. Négrier, P. Bordet, C. Etrillard, D. Mondieg, S. Pechev, E. Lebraud, J.-F. Létard, P. Guionneau, Crystal structures and spin crossover in the polymeric material $[\text{Fe}(\text{Htrz})_2(\text{trz})](\text{BF}_4)$

- including coherent-domain size reduction effects, *Eur. J. Inorg. Chem.* 2013, 796–802.
- 13 J. G. Haasnoot, G. Vos, W. L. Groeneveld, 1,2,4-triazole complexes III: complexes of transition metal(II) itrates and fluoroborates, *Z. Naturforsch B*, 1977, **32**, 1421–1430.
 - 14 J. Kröber, J.-P. Audière, R. Claude, E. Codjovi, O. Kahn, J. G. Haasnoot, F. Grolière, C. Jay, A. Bousseksou, J. Linares, F. Varret, A. Gonthier-Vassal, Spin transition and thermal hystereses in the molecular-based materials $[\text{Fe}(\text{Htrz})_2\text{trz}](\text{BF}_4)$ and $[\text{Fe}(\text{Htrz})_3](\text{BF}_4)_2 \cdot \text{H}_2\text{O}$ (Htrz = 1,2,4-4H-triazole; trz = 1,2,4-triazolato), *Chem. Mater.*, 1994, **6**, 1404–1412.
 - 15 A. Grosjean, N. Daro, B. Kauffmann, A. Kaiba, J. F. Létard, P. Guionneau, The 1-D polymeric structure of the $[\text{Fe}(\text{NH}_2\text{trz})_3](\text{NO}_3)_2 \cdot n\text{H}_2\text{O}$ (with $n=2$) spin crossover compound proven by single crystal investigations, *Chem. Commun.*, 2011, **47**, 12382–12384.
 - 16 (a) L. Moulet, N. Daro, C. Etrillard, J.-F. Létard, A. Grosjean and P. Guionneau, Rational control of spin crossover particle sizes: from nano- to micro-rods of $[\text{Fe}(\text{Htrz})_2\text{trz}](\text{BF}_4)$, *Magnetochemistry*, 2016, **2**, 10; (b) D. Mader, S. Pillet, C. Carteret, M.-J. Stébé and J.-L. Blin, Confined growth of spin crossover nanoparticles in surfactant-based matrices: enhancing shape anisotropy, *J. Dispers. Sci. Technol.* 2011, **32**, 1771–1779.
 - 17 E. Coronado, J. R. Galán-Mascarós, M. Monrabal-Capilla, J. García-Martínez and P. Pardo-Ibáñez, Bistable spin crossover nanoparticles showing magnetic thermal hysteresis near room temperature, *Adv. Mater.*, 2007, **19**, 1359–1361. C. Bartual-Murgui, E. Natividad and O. Roubeau, *J. Mater. Chem. C*, **2015**, **3**, 7916–7924
 - 18 H. Peng, G. Molnár, L. Salmon and A. Bousseksou, Spin crossover nano- and micrometric rod-shaped particles synthesized in homogeneous acid media, *Eur. J. Inorg. Chem.*, 2015, 3336–3342.
 - 19 A. Enriquez-Cabrera, A. Rapakousiou, M. Piedrahita Bello, G. Molnar, L. Salmon, A. Bousseksou, Spin crossover polymer composites, polymers and related soft materials, *Coord. Chem. Rev.*, 2020, **419**, 213396/1–23.
 - 20 (a) C. Faulmann, J. Chahine, I. Malfant, D. de Caro, B. Cormary, L. Valade, A facile route for the preparation of nanoparticles of the spin crossover complex $[\text{Fe}(\text{Htrz})_2\text{trz}](\text{BF}_4)$ in xerogel transparent composite films, *Dalton Trans.*, 2011, 2480–2485; (b) G. Molnár, S. Rat, L. Salmon, W. Nicolazzi and A. Bousseksou, Spin crossover nanomaterials: from fundamental concepts to devices, *Adv. Mater.*, 2018, **30**, 17003862/1–23.
 - 21 D. Qiu, L. Gu, X. L. Sun, D. H. Ren, Z. G. Gu and Z. Li, $\text{SCO}@\text{SiO}_2@\text{Au}$ core-shell nanomaterials: enhanced photo-thermal plasmonic effect and spin crossover properties, *RSC Adv.*, 2014, **4**, 61313–61319.
 - 22 I. Suleimanov, J. Sánchez Costa, G. Molnár, L. Salmon and A. Bousseksou, The photothermal plasmonic effect in spin crossover@silica-gold nanocomposites, *Chem. Commun.*, 2014, **50**, 13015–13018.
 - 23 (a) L. Moulet, N. Daro, S. Mornet, N. Vilar-Vidal, G. Chastanet and P. Guionneau, Grafting of gold onto spin crossover nanoparticles: $\text{SCO}@\text{Au}$, *Chem. Commun.*, 2016, **52**, 13213–13216; (b) M. Palluel, N. M. Tran, N. Daro, S. Buffière, S. Mornet, E. Freysz and G. Chastanet, The interplay between surface plasmon resonance and switching properties in gold@spin crossover nanocomposites, *Adv. Funct. Mater.*, 2020, **30**, 2000447/1–9.
 - 24 V. Y. Sirenko, O. I. Kucheriv, A. Rotaru, I. O. Fritsky and I. A. Gural'skiy, Direct synthesis of spin crossover complexes: an unexpectedly revealed new iron-triazolic structure, *Eur. J. Inorg. Chem.*, 2020, **2020**, 4523–4531.
 - 25 (a) J. H. Askew and H. J. Shepherd, Mechanochemical synthesis of cooperative spin crossover materials, *Chem. Commun.*, 2018, **54**, 180–183; (b) J. H. Askew, D. M. Pickup, G. O. Lloyd, A. V. Chadwick and H. J. Shepherd, Exploring the effects of synthetic and postsynthetic grinding on the properties of the spin crossover material $[\text{Fe}(\text{atrz})_3](\text{BF}_4)_2$ (atrz = 4-amino-4H-1,2,4-triazole), *Magnetochemistry*, 2020, **6**, 1–12; (c) J. H. Askew and H. J. Shepherd, Post-synthetic anion exchange in iron(II) 1,2,4-triazole based spin crossover materials via mechanochemistry, *Dalton Trans.*, 2020, **49**, 2966–2971.
 - 26 N. Daro, L. Moulet, N. Penin, N. Paradis, J.-F. Létard, E. Lebraud, S. Buffière, G. Chastanet and P. Guionneau, Spray-drying to get spin crossover materials, *Materials*, 2017, **10**, 60.
 - 27 C. C. W. K. Robertson, P.B. Flandrin, H.J. Shepherd, $[\text{Fe}(\text{Htrz})_2\text{trz}](\text{BF}_4)$ nanoparticle production in a milli-scale segmented flow crystalliser, *Chim. Oggi-Chem. Today*, 2017, **35**, 19.
 - 28 N. Daro, T. Vaudel, L. Afindouli, S. Marre, C. Aymonier and G. Chastanet, ONE-step synthesis of spin crossover nanoparticles using flow chemistry and supercritical CO_2 , *Chem. – A Eur. J.*, 2020, 16286–16290.
 - 29 K. Sugiyarto and H. Goodwin, Cooperativ spin transition in iron(II) derivatives of 1,2,4-triazole, *Aust. J. Chem.*, 1994, **47**, 263.
 - 30 A. Boulouf and D. Louër, *J. Appl. Crystallogr.*, 2004, **37**, 724–731.
 - 31 O. Kahn, J. Kröber and C. Jay, Spin transition molecular materials for displays and data recording, *Adv. Mater.*, 1992, **4**, 718–728.
 - 32 A. Michalowicz, J. Moscovici, B. Ducourant, D. Cracco and O. Kahn, EXAFS and X-ray powder diffraction studies of the spin transition molecular materials $[\text{Fe}(\text{Htrz})_2\text{trz}](\text{BF}_4)$ and $[\text{Fe}(\text{Htrz})_3](\text{BF}_4)_2 \cdot \text{H}_2\text{O}$ (Htrz = 1,2,4-4H-triazole; trz = 1,2,4-triazolato), *Chem. Mater.*, 1995, **7**, 1833–1842.
 - 33 D. Nieto-Castro, F. A. Garcés-Pineda, A. Moneo-Corcuera, B. Pato-Doldan, F. Gispert-Guirado, J. Benet-Buchholz and J. R. Galán-Mascarós, Effect of mechanochemical recrystallization on the thermal hysteresis of 1D Fe^{II} -triazole spin crossover polymers, *Inorg. Chem.*, 2020, **59**, 7953–7959.
 - 34 S. A. Siddiqui, O. Domanov, E. Schafner, J. Vejpravova and H. Shiozawa, Synthesis and size-dependent spin crossover of coordination polymer $[\text{Fe}(\text{Htrz})_2\text{trz}](\text{BF}_4)$, *J. Mater. Chem. C*, 2021, **9**, 1077–1084.